Analytica Chimica Acta 788 (2013) 24–31

Contents lists available at SciVerse ScienceDirect

Analytica Chimica Acta

journal homepage: www.elsevier.com/locate/aca

A novel electrochemical biosensor based on the hemin-graphene nano-sheets and gold nano-particles hybrid film for the analysis of hydrogen peroxide

Haiyan Song[a,b], Yongnian Ni[a,b,*], Serge Kokot[c]

[a] State Key Laboratory of Food Science and Technology, Nanchang University, Nanchang 330031, China
[b] Department of Chemistry, Nanchang University, Nanchang 330031, China
[c] School of Chemistry, Physics and Mechanical Engineering, Science and Engineering Faculty, Queensland University of Technology, Brisbane, 4001, Australia

HIGHLIGHTS

- Synthesis of a new biological material-hemin-graphene.
- Construction of a novel hemin-graphene/gold nanoparticles biosensor.
- The biosensor showed excellent electrocatalytic activity toward hydrogen peroxide.
- The process of constructing the biosensor is easy and quick.
- The biosensor has a high sensitivity and low detection limit.

GRAPHICAL ABSTRACT

A novel hemin-graphene nano-sheets (H-GNs)/gold nano-particles (AuNPs) electrochemical biosensor was constructed for analysis of hydrogen peroxide. Due to the synergy effect of H-GNs and AuNPs, the biosensor showed a satisfactory electrocatalytic activity for the reduction of hydrogen peroxide.

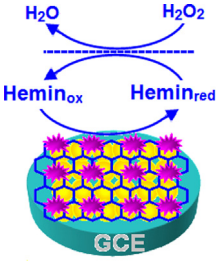

ARTICLE INFO

Article history:
Received 30 April 2013
Received in revised form 14 June 2013
Accepted 16 June 2013
Available online 20 June 2013

Keywords:
Hemin-graphene nano-sheets
Gold nano-particles
Hybrid film
Hydrogen peroxide
Electrocatalysis

ABSTRACT

Hydrogen peroxide is an important analyte in biochemical, industrial and environmental systems. Therefore, development of novel rapid and sensitive analytical methods is useful. In this work, a hemin-graphene nano-sheets (H-GNs)/gold nano-particles (AuNPs) electrochemical biosensor for the detection of hydrogen peroxide (H_2O_2) was researched and developed; it was constructed by consecutive, selective modification of the GCE electrode. Performance of the H-GNs/AuNPs/GCE was investigated by chronoamperometry, and AFM measurements suggested that the graphene flakes thickness was ~1.3 nm and that of H-GNs was ~1.8 nm, which ultimately indicated that each hemin layer was ~0.25 nm. This biosensor exhibited significantly better electrocatalytic activity for the reduction of hydrogen peroxide in comparison with the simpler AuNPs/GCE and H-GNs/GCE; it also displayed a linear response for the reduction of H_2O_2 in the range of 0.3 μM to 1.8 mM with a detection limit of 0.11 μM ($S N^{-1} = 3$), high sensitivity of 2774.8 $\mu A\, mM^{-1}\, cm^{-2}$, and a rapid response, which reached 95% of the steady state condition within 5 s. In addition, the biosensor was unaffected by many interfering substances, and was stable over time. Thus, it was demonstrated that this biosensor was potentially suitable for H_2O_2 analysis in many types of sample.

1. Introduction

Nano-materials have unique photonic, electronic, magnetic, electrocatalytic and biosensing properties, which have been recently exploited successfully [1–5]. In this context, gold nanoparticles (AuNPs) have been studied extensively because they

* Corresponding author at: Department of Chemistry, Nanchang University, Nanchang 330031, China. Tel.: +86 791 83969500; fax: +86 791 83969500.
E-mail addresses: ynni@ncu.edu.cn (Y. Ni), s.kokot@qut.edu.au (S. Kokot).

0003-2670/$ – see front matter © 2013 Elsevier B.V. All rights reserved.
http://dx.doi.org/10.1016/j.aca.2013.06.016

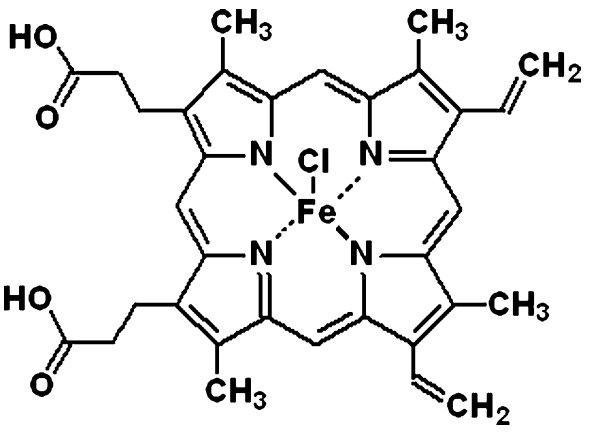

Scheme 1. Molecular structure of the hemin.

have high biocompatibility, good conductivity and satisfactory catalytic activity; this range of properties are particularly useful for the application of AuNPs in the construction of electrochemical biosensors [6–9]. A common method for making AuNPs is electrodeposition, which enables fine-tuning and fast response of the nano-material systems to changes in deposition conditions; at the same time the procedure is simple and rapid [10–12].

Graphene is a standard, two-dimensional (2D), one-atom-thick sheet material with interesting physical and chemical properties [13,14]. Its unique structure and properties, such as high specific surface area, high mechanical strength and conductivity as well as its relatively low price make graphene suitable for potential applications, for example, field-effect transistors, gas sensors, and batteries [15–20]. Graphene, obtained from the reduction of graphene oxide (GO), can be processed, and new functional groups such as carboxylic groups, can be inserted; these particular groups facilitate GO's dispersion in an aqueous solution [21]. Other useful properties can be obtained from non-covalent functionalization, for example: the binding of molecules through π–π stacking or via hydrophobic interactions; importantly, there is no loss of the intrinsic properties of graphene [22]. Thus, the modified materials, produced in this way, combine the advantages of graphene and the attached molecules. Huang et al. prepared a composite hydrogel containing graphene oxide and hemoglobin, and used this hydrogel as a catalyst for the oxidation of pyrogallol; this composite material has considerably improved the catalytic activity and stability during the oxidation reaction [23]. Also, graphene has significant potential as a supporting material for immobilizing and stabilizing metal nanoparticles, for the development of new electro-catalysis systems [24].

Hemin (iron protoporphyrin IX), or heme in its oxidized state (Scheme 1), is a well known natural metaloporphyrin and is the active site in heme-proteins, such as catalases, peroxidases, hemoglobins and myoglobins [25]. It can be used as an electron source based on the reversible Fe(III)/Fe(II) redox couple, which exhibits strong electrocatalytic properties in the presence of many small molecules such as nitrite [26], oxygen [27], nitric oxide [28], L-tyrosine [29] and hydrogen peroxide [30]. In addition, it shows peroxidase-like activity, which, through the catalytic involvement of H_2O_2, oxidizes the substrate to produce a change in color [31]. However, direct application of hemin as a catalyst is difficult because it is sparingly soluble; also, its molecular aggregation in aqueous solution to form catalytically inactive dimers, and its destruction in the oxidizing media, both weaken its catalytic activity [32]. Thus, to overcome this problem, functional porphyrin derivatives are particularly useful for the synthesis of functional materials such as hemin-graphene hybrid nano-sheets (H-GNs), which utilize π–π interactions [33,34]. In this case, graphene, as a support for hemin molecules, not only provides high thermal and electrical conductivities but also maintains the intrinsic characteristics of hemin.

In general, in nature, H_2O_2 is often associated with different biological processes, particularly in various waterways where it often acts as a strong, non-polluting oxidant producing water as its important reaction product; however, it should be noted that other by-products include highly reactive, short-life radicals, which are often damaging to the surroundings. Also, H_2O_2 is utilized in many industrial processes such as the manufacture of pharmaceuticals, treatment of paper, textiles and food, mostly as a bleaching or cleaning agent [35,36]. Additionally, it is used as a rocket propellant. Therefore, analysis of H_2O_2 is of considerable importance in natural and industrial samples.

In this work, the GCE was modified firstly with the deposition of the gold nanoparticles, followed by the graphene layer and finally, by a monolayer of hemin, which became attached to the graphene by means of physical crosslinks. Thus, the hemin-graphene system ultimately formed a composite hydrogel, which can provide an aqueous micro-environment to protect the activity of, for example, the hemin. The gold nano-particles, which have a large surface area and good conductivity, enable the loading of a large amount of H-GNs and the promotion of electron transfer. Thus, this layer-by-layer H-GNs/AuNPs/GCE structure significantly improved the electrocatalytic activity and the electrochemical stability for the determination of hydrogen peroxide.

The aims of this work were: (1) to construct a new H-GNs/AuNPs/GCE by electrodepositing the gold nano-particles onto the GCE followed by the deposition of the H-GNs onto this modified electrode; (2) to investigate the electrochemical and electrocatalytic performance of H-GNs/AuNPs/GCE, H-GNs/GCE and AuNPs/GCE, particularly for the analysis of H_2O_2, with the use of cyclic voltammetry (CV) and the electrochemical impedance spectroscopy (EIS); and (3) to investigate the potential of this biosensor for the quantitative analysis of H_2O_2.

2. Experimental

2.1. Reagents

Graphite powders of spectroscopic purity were purchased from Shanghai Chemical Reagent Co., Shanghai, China; Hemin and Hydrogen tetrachloroaurate tetrahydrate ($HAuCl_4{\cdot}4H_2O$) were obtained from Sigma–Aldrich Co., U.S.; Hydrogen peroxide solution (30 wt.% in H_2O) and other reagents were purchased from Shanghai Chemical Reagent Co., Shanghai, China. Unless otherwise stated, the chemicals in this work were all Analytical Grade reagents; they were used as received without further purification. Diluted H_2O_2 solution was freshly prepared before use. Phosphate buffer solution (PBS, 0.05 M, pH 7.44) was the supporting electrolyte, and was prepared from KH_2PO_4 and K_2HPO_4 salts. Twice-distilled water was used throughout the experiments.

2.2. Instruments

Atomic force microscopy (AFM) measurements were carried out with an AJ-III AFM system (Shanghai Aijian Nanotechnology) in the tapping mode. Standard silicon (Si) cantilevers (spring constant, 0.6–6 Nm^{-1}) were used at its resonance frequency (typically 60–150 kHz). All AFM images were acquired at room temperature under ambient conditions.

The morphology of the modified electrodes was investigated with the use of a Scanning electron microscope (SEM; Hitachi S-3000N, Hitachi, Japan). The operational power was 20.0 kV, and the magnification for all samples was 13,000.

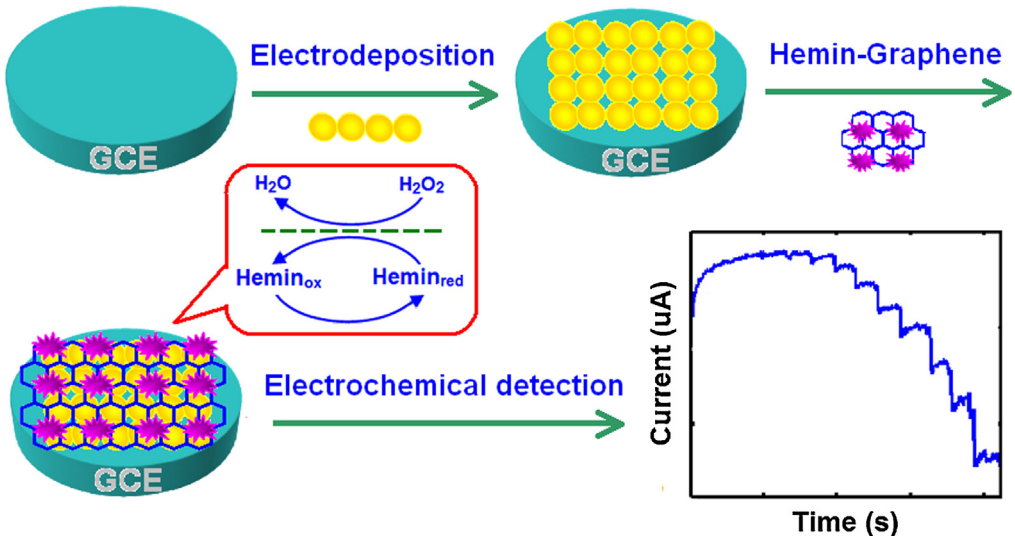

Scheme 2. Preparation of the H-GNs/AuNP/GCE biosensor for the analysis of hydrogen peroxide followed by the electrochemical detection process and the output.

UV–vis absorption spectra were recorded on an Agilent 8453 UV–vis spectrometer in the range of 200–800 nm (Agilent Technologies, Inc., U.S.A.).

All electrochemical experiments were performed on a CHI-660A electrochemical workstation (Shanghai Chenhua Apparatus Co., Shanghai, China) in conjunction with a standard three-electrode system: the working electrode–either the original or the modified GCE (d = 3 mm), the counter electrode – a platinum wire, and the reference electrode – an Ag/AgCl (sat. NaCl). A cell stand (Model BAS C1A, U.S.) was used for voltammetric scanning and to stir the test solution during the experiment. Also, the EIS experiments for the modified GCE were performed in 0.1 mol L^{-1} KCl containing 5×10^{-3} mol L^{-1} $[Fe(CN)_6]^{-3/-4}$ (1:1) solution with the use of the CHI-660A electrochemical workstation.

2.3. Preparation of the H-GNs/AuNPs modified electrode

2.3.1. Synthesis of graphene and H-GNs

Graphene oxide (GO) was synthesized from natural graphite by the Hummers and Offeman method, which was slightly modified [21]. H-GNs were prepared according to the literature [22,37]. Generally, 20.0 mL of the homogeneous GO dispersion (0.5 mg mL^{-1}) were mixed with 20.0 mL 0.5 mg mL^{-1} hemin solution and 200.0 μL ammonia solution (25%), followed by the addition of 30.0 μL hydrazine solution. After vigorous shaking or stirring for a few minutes, the beaker was placed in a water bath (60 °C) for 3.5 h. A stable black dispersion was obtained. This dispersion was filtered off on a nylon membrane (0.22 μm) so as to obtain H-GNs that can be redispersed readily in water by ultrasonication.

2.3.2. Preparation of the H-GNs/AuNPs/GCE, H-GNs/GCE and AuNPs/GCE modified electrodes

The glassy carbon electrode (GCE, d = 3 mm) was polished to a mirror shine with 0.1 and 0.05 μm alumina slurry, sequentially, and then, it was sonicated, in turn, in nitric acid (1:1), ethanol and doubly distilled water. After the electrodes were dried in air, they were dipped into a 0.024 M $HAuCl_4$ solution under static conditions and the AuNPs were electrodeposited for 20 s at a constant potential of −0.2 V to obtain the AuNPs/GCE. The H-GNs/GCE and H-GNs/AuNPs/GCE were constructed by spreading 15 μL of an H-GNs suspension onto the surface of a well-polished GCE and that of the modified electrode. Finally, the modified electrodes were activated by several successive scans with a scan rate of 100 mV s^{-1} in the PBS buffer solution (pH 7.44) until a constant voltammogram was obtained. A schematic illustration of the stepwise procedure and electrochemical detection of the biosensor was presented in Scheme 2.

3. Results and discussion

3.1. Characterization of the H-GNs

The morphology and thickness of the H-GNs were investigated with the use of the atomic force microscopy (AFM). Specifically, graphene was first deposited onto a silicon oxide substrate from an aqueous solution. AFM images were taken and then used to determine the thickness of the selected graphene flakes (approximately 1.3 nm for two to three layers of graphene (Fig. 1A (a)). The average thickness of H-GNs was approximately 1.8 nm (Fig. 1A (b)). Thus, there was an increase of 0.5 nm in the thickness of the H-GNs compared to that of the unmodified graphene; this change was attributed to the presence of hemin on the surfaces of the graphene. Since hemin could be located on both sides of the graphene layer, then the thickness of a hemin layer on graphene should be about 0.25 nm. This result is consistent with that previously reported [22]. When the thickness of the hemin layer on the graphene was compared with that of a single hemin molecule (0.2 nm), it is reasonable to suggest that the graphene nano-sheets were covered by a monolayer of hemin. Successful synthesis of H-GNs was also confirmed with the use of UV–vis spectroscopy (Fig. 1B). A spectrum of the hemin solution (Fig. 1B, curve a) was characterized by a strong peak at 385 nm, which was attributed to the Soret band; also, there was a group of weak peaks between 500 and 700 nm, which were attributed to the Q-bands. The GO dispersion (Fig. 1B, curve b) showed a maximum absorption at 228 nm, which was assigned to the π–π* transition of the aromatic C=C bonds, and the shoulder at 280–320 nm was assigned to the n–π* transition of the C=O bond [33]. The H-GNs spectrum (Fig. 1B, curve c) had a peak absorption at 265 nm, which was in close agreement with that observed for the reduced graphene oxide [33]. The remaining spectral features characterized by the absorption at 415 nm were assigned to the Soret band of hemin allowing for a large bathochromic shift (30 nm). This last band assignment was supported by a study of the interaction of a cationic porphyrin derivative with chemically converted graphene, which similarly displayed a red shift of the porphyrin Soret band [33]. Thus, this interpretation of the UV–vis spectra of

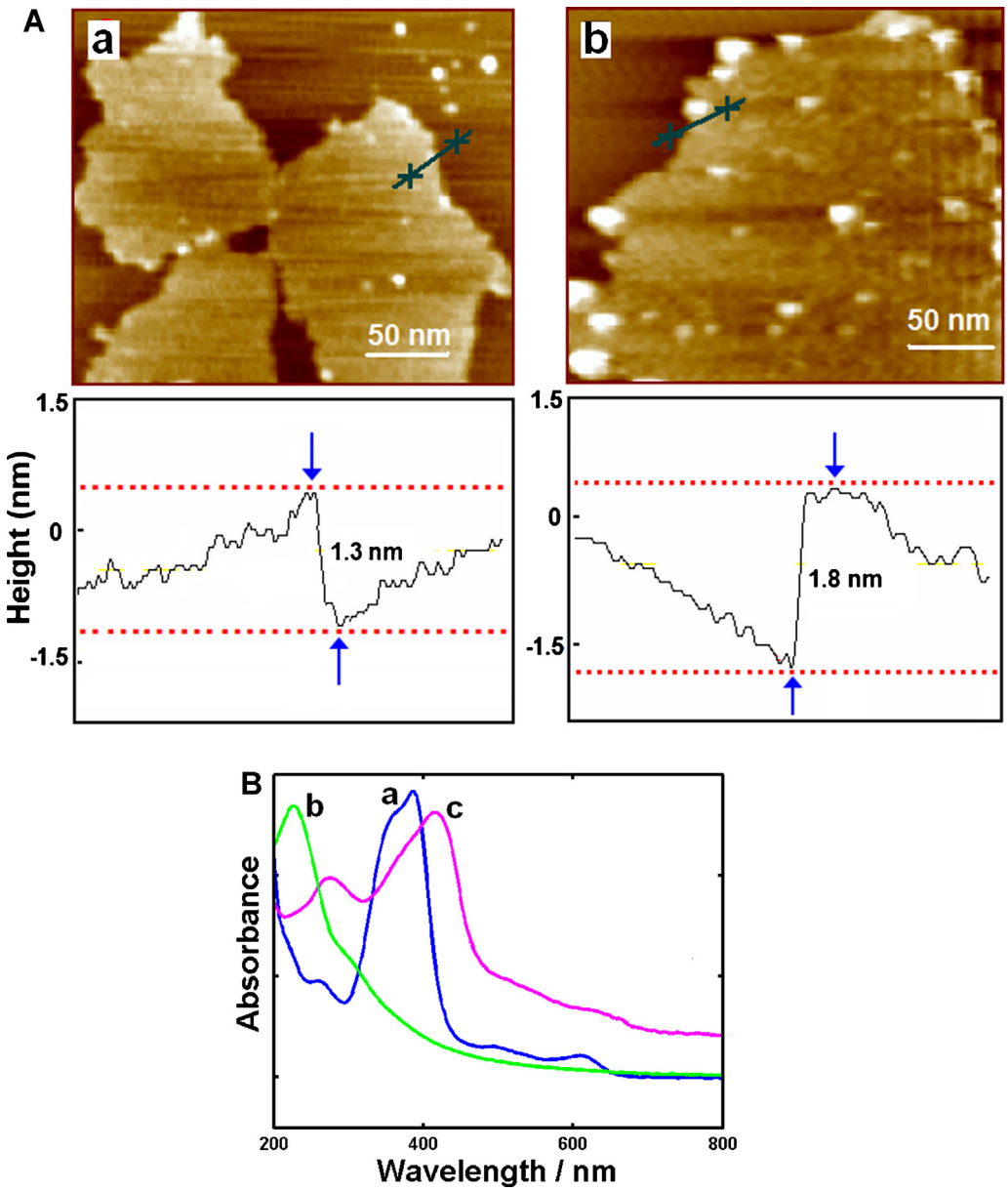

Fig. 1. (A) AFM images of (a) graphene, and (b) the H-GNs. (B) UV–vis absorption spectra of (a) hemin solution, (b) GO suspension, and (c) H-GNs suspension.

the H-GN system strongly indicated that the hemin molecules were attached to the graphene. The coverage of graphene by hemin was calculated to be about 19.9%; this was established by comparing the absorbance of H-GNs with that of hemin.

3.2. Characterization of the deposited AuNPs as a function of the electrodeposition time

During the electrodeposition process, the deposition time can affect the morphology and distribution of the nano-particles [38]. The state of the AuNPs deposited for different electrodeposition times 10, 20 and 40 s, were investigated with the use of the SEM technique. When the deposition time was 10 s, the distribution of the nano-particles was uneven and sparse (Fig. 2A). When the time was increased to 20 s, the amount of the nano-particles increased, and the particle size and distribution were observed to be quite uniform (Fig. 2B). After a 40 s deposition period, the number of the particles increased even more, but the size distribution was uneven, particularly with the appearance of quite a few large particles (Fig. 2C). Thus, 20 s was selected as the optimal deposition time, and in this case, the average diameter of the AuNPs was about 40 nm.

3.3. Electrochemical impedance spectroscopy and cyclic voltammetry characterization of the modified electrodes

Voltammograms from differently modified electrodes immersed in a 1:1 mixture of 5×10^{-3} mol L^{-1} $[Fe(CN)_6]^{-3/-4}$ solution and 0.1 mol L^{-1} KCl, were obtained with the use of cyclic voltammetry (CV; Fig. 3A). The $[Fe(CN)_6]^{-3/-4}$ complex ions are electrochemical probes commonly utilized for the investigation of the construction of complex biosensors [29]. Well-defined oxidation and reduction peaks of $[Fe(CN)_6]^{-3/-4}$ (Fig. 3A, curve a) were observed at the untreated GCE. After the AuNPs were deposited on the electrode, the peak current at the modified electrode increased (Fig. 3A, curve b). This was attributed to the good conductivity of the AuNPs; this could facilitate electron transfer between the nano-particles and the electrode surface. In contrast,

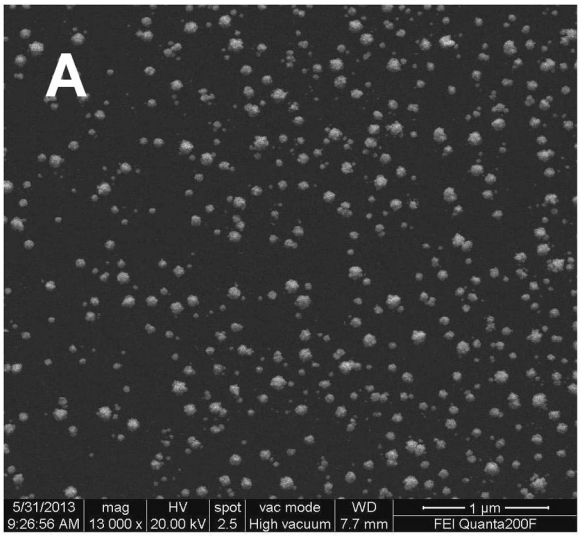

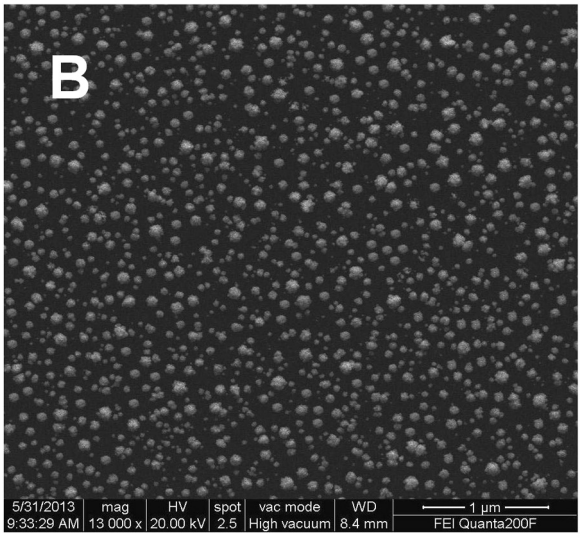

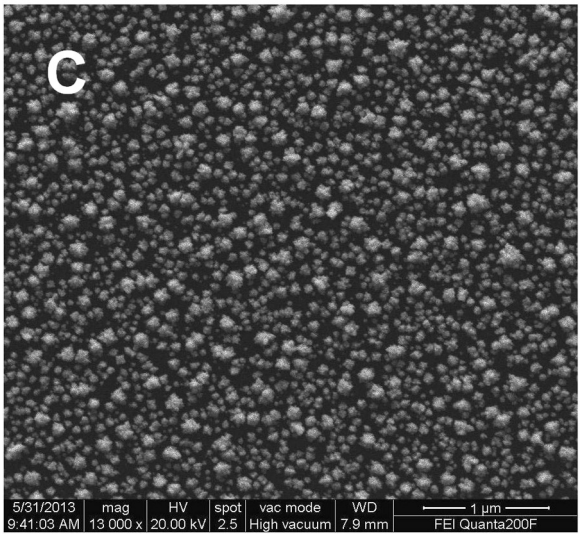

Fig. 2. SEM images of AuNPs at different deposition times: (A) 10 s, (B) 20 s, and (C) 40 s.

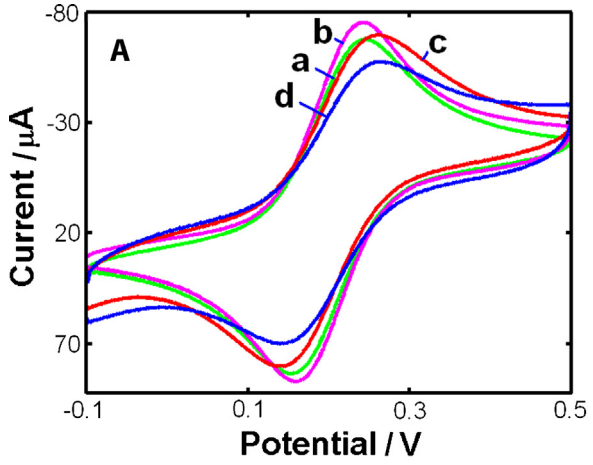

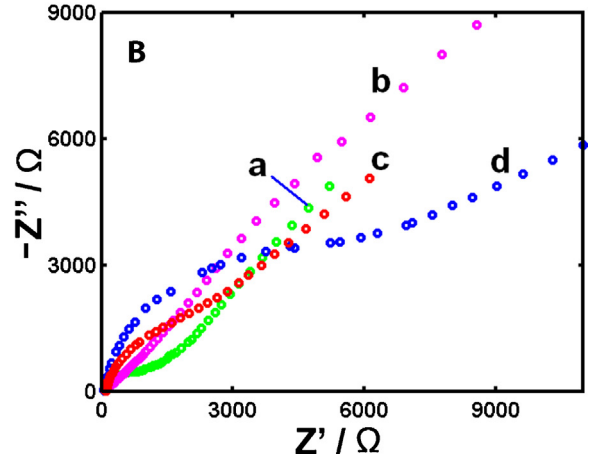

Fig. 3. Results from: (A) Cyclic voltammograms (CVs), and (B) Electrochemical impedance spectroscopy (EIS) of the different electrodes in 1:1 5 mM $[Fe(CN)_6]^{-3/-4}$/0.1 M KCl solutions. Curves: a – GCE (green), b – AuNPs/GCE (mauve), c – H-GNs/GCE (red), and d – H-GNs/AuNPs/GCE (blue) (For interpretation of the references to colour in this figure legend, the reader is referred to the web version of this article.)

when the GCE was treated only with the H-GNs, the reversibility decreased compared with the untreated GCE (Fig. 3A, curve c). This demonstrated that the H-GNs somehow impede the electron transfer between the bio-molecules and the electrode surface [33]. However, when the H-GNs and AuNPs were both deposited on the GCE, the cathodic and anodic peak currents clearly decreased (Fig. 3A, curve d). This may be attributed to the thickness of the membrane, which could hinder the electron transfer [39].

EIS is another well known method for studying interface properties of different modified electrodes [40]. It was also used to investigate the stepwise assembly of the biosensor. Generally, there are two types of result often observed on an EIS plot: the first is a semicircular graph found at higher frequencies, and this is related to the electron transfer-limited processes in a film; the second is a linear graph found at lower frequencies, and is related to the diffusion-limited processes in a film. Additionally, in the former case, the diameter of the semicircular plot is proportional to the electron-transfer resistance. Thus, in this study, the untreated GCE produced an essentially linear EIS plot with, arguably, a slight, initial curvature (Fig. 3B, curve a). When the AuNPs were electrodeposited on the GCE, the plot was effectively linear possibly because the AuNPs are good electron conductors (Fig. 3B, curve b). However, when the H-GNs/GCE was tested, the EIS initially produced a definite, significant curvature followed by essentially a linear plot, which suggested that

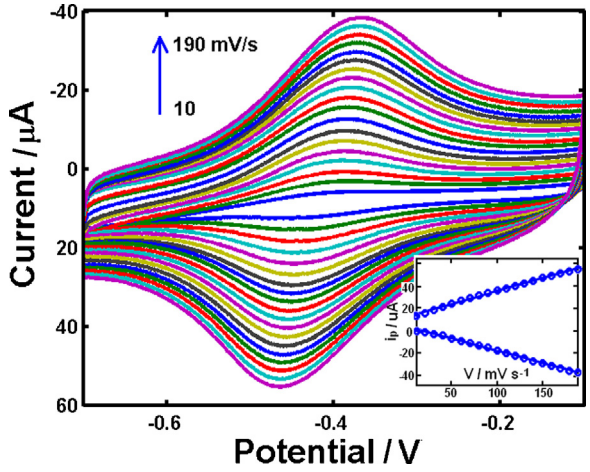

Fig. 4. Cyclic voltammograms obtained by the novel H-GNs/AuNPs/GCE in 0.05 M KH_2PO_4/K_2HPO_4 buffer (pH 7.44) at various scan rates measured at 10, 20, . . ., 190 mV s^{-1} (from inner to outer profiles), respectively. Insert: plots of peak currents vs. scan rates.

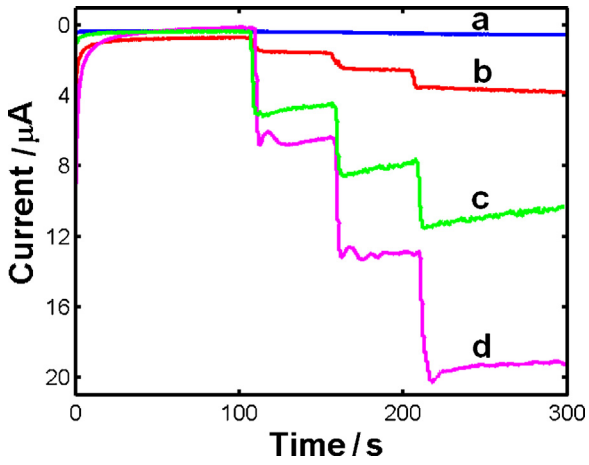

Fig. 5. Amperometric responses recorded at the GCE (curve a, blue); AuNPs/GCE (curve b, red); H-GNs/GCE (curve c, green) and H-GNs/AuNPs/GCE (curve d, mauve); analyses of several consecutive responses are shown from successive additions of 0.05 mM H_2O_2 dissolved in 0.05 M KH_2PO_4/K_2HPO_4 buffer (pH 7.44) saturated with N_2 gas (For interpretation of the references to colour in this figure legend, the reader is referred to the web version of this article.)

the electron transfer resistance increased (Fig. 3B, curve c). The H-GNs/AuNPs/GCE complete electrode assembly produced an EIS plot, which initially indicated a strongly curved profile, which then effectively straightened out (Fig. 3B, curve d); this suggested that electron transfer was inhibited, presumably because of the increase in the thickness of the surface layers. It is notable that these results are consistent with those from the CV work described above.

The H-GNs/AuNPs/GCE was also investigated with the use of the CV technique using different scan rates (Fig. 4). With increasing scan rate, both redox peak currents and peak-to-peak separation increased, and the anodic and cathodic peak currents were linearly proportional to the scan rate ranging from 10 to 190 mV s^{-1}; (Fig. 4, Insert); this indicated that the behavior of the biosensor was a surface-confined process [37].

3.4. Electrocatalysis of H_2O_2 at the H-GNs/AuNPs/GCE

To investigate the performance of the four different types of electrode, amperometric experiments were conducted at each electrode immersed in 0.05 mM H_2O_2 in 0.05 M KH_2PO_4/K_2HPO_4 buffer (pH 7.44), which was stirred and saturated by the bubbling N_2 gas (Fig. 5: GCE (curve a), AuNPs/GCE (curve b), and H-GNs/GCE (curve c)). The results indicated that H_2O_2 reduction was barely present at the untreated GCE. However, the catalytic current at the AuNPs/GCE and also at the H-GNs/GCE significantly increased relative to that measured at the untreated GCE. This observation may reflect the strong catalytic effect of the AuNPs and the nature of the peroxidase in the hemin of the H-GNs. A much larger current response was observed at the H-GNs/AuNPs/GCE; this significant improvement could be attributed to the synergistic catalytic effect of H-GNs and AuNPs.

Similar experiments were conducted at the H-GNs/AuNPs/GCE but different aliquots of H_2O_2 were added to the stirred electrolyte solution at −0.2 V (Fig. 6A). When the analyte was added to the electrochemical cell, a rapid increase in the reduction current was observed; within 5 s this reached a level of 95% of the steady-state current. The current response increased linearly with the concentration of H_2O_2 (Fig. 6B), and this plot could be used as a calibration curve for the analysis of H_2O_2 at the modified electrode (concentration range: 0.0003–1.8000 mM). The calibration equation was: $I(\mu A) = 13.34 + 196.04\ c(mM)$, with a correlation coefficient of 0.998. The sensitivity of the modified electrode was 2774.8 μA mM^{-1} cm^{-2} H_2O_2 with a detection limit 0.11 μM at the signal-to-noise ratio of 3.

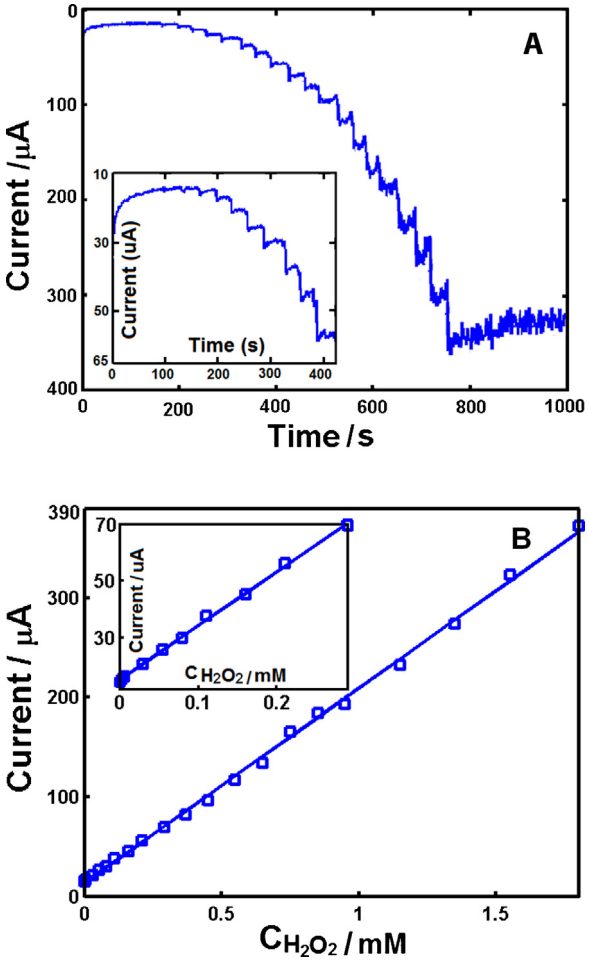

Fig. 6. (A) Amperometric responses recorded at the H-GNs/AuNPs/GCE from successive additions of H_2O_2 dissolved in 0.05 M KH_2PO_4/K_2HPO_4 buffer (pH 7.44), which was saturated with N_2 gas. Applied potential: −0.2 V (vs. SCE). Inset: Magnified plot of the weaker responses (0–400 s). (B) Calibration curve of the H-GNs/AuNPs modified electrode as a function of hydrogen peroxide concentration. Inset: Magnified plot of the low H_2O_2 concentrations (0.00–0.29 mM).

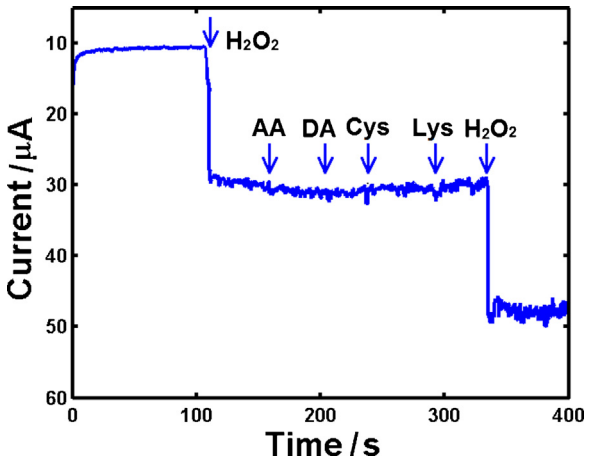

Fig. 7. Results of the effect of potential interference agents; these were added to the solution sequentially: 0.1 mM H_2O_2, 1 mM ascorbic acid (AA), 1 mM dopamine (DA), 1 mM cysteine (Cys), 1 mM lysine (Lys), and 0.1 mM H_2O_2 (the stirred sample solution was a 0.05 M KH_2PO_4/K_2HPO_4 buffer (pH 7.44) saturated with N_2 gas.).

3.5. Selectivity and other properties of the modified electrode

In previous work [41], simultaneous electro-oxidation of potential interferences such as ascorbic acid and cysteine were reported as a drawback of the amperometric detection of the H_2O_2 analyte. In this work, the amperometric response of the biosensor to the consecutive addition of 0.1 mM H_2O_2 and 1 mM interfering substances was investigated; the interfering substances included ascorbic acid (AA), dopamine (DA), cysteine (Cys) and lysine (Lys). It was evident from the trace of the response current that the influence of the tested interfering species on the response of the H_2O_2 was negligible (Fig. 7); this observation indicated that the novel biosensor was highly selective for the analyte, and because its operating potential range was closer to the redox potential of the hemin, there was a decrease in responses from any interfering reactions [42].

The reproducibility of the constructed biosensor was also researched. Thus, when four consecutive current measurements of a 1 mM H_2O_2 solution were recorded at the biosensor, the relative standard deviation (RSD) was ±3.8%. Similarly, when four separate electrodes were immersed in the above analyte solution under the same conditions, the RSD for electrode-to-electrode reproducibility of these four electrodes was ±5.2%. In addition, the stability of the modified electrode as a function of time was studied over several weeks by the discontinuous measurement of the current responses from the reduction reaction of H_2O_2 while the biosensor was stored at 4 °C. There were no significant changes to the current response observed during the first three days. After the biosensor was stored for two weeks and then a month, it retained 93.1% and 83.4% of its original sensitivity. These results indicated that the stability of the electrodes and the reproducibility of the analysis of H_2O_2 were satisfactory; such performance was facilitated by the high levels of conductivity of the AuNPs, which indicated that the structure of the biosensor, although complex, did lead to an improved electron-transfer. In addition, the nano-particles enlarged the specific surface area of the electrode, and provided for increased loading of the H-GNs.

4. Conclusions

A novel biosensor was successfully fabricated with the use of a GCE electrode, which was modified with the AuNPs and H-GNs. This H-GNs/AuNPs/GCE biosensor showed a better electrocatalytic activity for the reduction of H_2O_2 compared with the AuNPs/GCE, H-GNs/GCE, and GCE. It was confirmed that the increased catalytic response was due to the enlarged specific surface area of the electrode, and the higher loading of the H-GNs; hence, an improved synergistic catalytic effect was observed between the AuNPs and H-GNs. The satisfactory performance of the biosensor was attributed to its high sensitivity, good stability and reproducibility, wide linear response range, short response time and high analyte specificity. Therefore, this biosensor is particularly useful for analysis of the important hydrogen peroxide analyte in many systems buffered at pH 7.44 in 0.05 M KH_2PO_4/K_2HPO_4 within the analyte concentration range of 0.0003–1.8000 mM.

Acknowledgements

The authors gratefully acknowledge the financial support of this study by the National Natural Science Foundation of China (NSFC-21065007), the Education Department Science Foundation of Jiangxi Province (GJJ10037), and the State Key Laboratory of Food Science and Technology of Nanchang University (SKLF-ZZA-201302 and SKLF-ZZB-201303).

References

[1] S.N. Ding, B.H. Gao, D. Shan, Y.M. Sun, S. Cosnier, Biosens. Bioelectron. 39 (2013) 342–345.
[2] J.Q. Tian, H.L. Li, W.B. Lu, Y.L. Luo, L. Wang, X.P. Sun, Analyst 136 (2011) 1806–1809.
[3] O. Akman, H. Kavas, A. Baykal, M.S. Toprak, Ali Coruh, B. Aktas, J. Magn. Magn. Mater. 327 (2013) 151–158.
[4] S.K. Annamalai, B. Palani, K.C. Pillai, Colloids Surf. A 395 (2012) 207–216.
[5] A. Balamurugan, K.C. Ho, S.M. Chen, T.Y. Huang, Colloids Surf. A 362 (2010) 1–7.
[6] F.F. Liang, C.Y. Liu, J. Jiao, S.Q. Li, J. Xia, J.B. Hu, Microchim. Acta 177 (2012) 389–395.
[7] J. Du, X.P. Yu, J.W. Di, Biosens. Bioelectron. 37 (2012) 88–93.
[8] K. Zhang, J. Wei, H.J. Zhu, F. Ma, S.H. Wang, Mater. Res. Bull. 48 (2013) 1338–1341.
[9] B.Z. Zheng, S.P. Xie, L. Qian, H.Y. Yuan, D. Xiao, M.M.F. Choi, Sens. Actuators B 152 (2011) 49–55.
[10] S.S. Kumar, J. Joseph, K.L. Phani, Chem. Mater. 19 (2007) 4722–4730.
[11] M.P. Ngoc Bui, X.H. Pham, K.N. Han, C.A. Li, E.K. Lee, H.J. Chang, G.H. Seong, Electrochem. Commun. 12 (2010) 250–253.
[12] M.C. Tsai, P.Y. Chen, Talanta 76 (2008) 533–539.
[13] L. Liu, S.M. Ryu, M.R. Tomasik, E. Stolyarova, N. Jung, M.S. Hybertsen, M.L. Steigerwald, L.E. Brus, G.W. Flynn, Nano Lett. 8 (2008) 1965–1970.
[14] C.N.R. Rao, A.K. Sood, K.S. Subrahmanyam, A. Govindaraj, Angew. Chem. Int. Ed. 48 (2009) 7752–7777.
[15] J. Lee, L. Tao, K.N. Parrish, Y.F. Hao, R.S. Ruoff, Appl. Phys. Lett. 101 (2012), 252109-1-4.
[16] D.J. Kim, I.Y. Sohn, J.H. Jung, O.K. Yoon, N.E. Lee, J.S. Park, Biosens. Bioelectron. 41 (2013) 621–626.
[17] X.Q. Lin, J. Ni, C. Fang, J. Appl. Phys. 113 (2013), 034306-1-6.
[18] C.W. Chen, S.C. Hung, M.D. Yang, C.W. Yeh, C.H. Wu, Appl. Phys. Lett. 99 (2011), 243502-1-3.
[19] M. Zhang, M.Q. Jia, Y.H. Jin, Appl. Surf. Sci. 261 (2012) 298–305.
[20] F. Kokai, R. Sorin, H. Chigusa, K. Hanai, A. Koshio, M. Ishihara, Y. Koga, M. Hasegawa, N. Imanishi, Y. Takeda, Diamond Relat. Mater. 29 (2012) 63–68.
[21] Y.Y. Jiang, X.D. Zhang, C.S. Shan, S.C. Hua, Q.X. Zhang, X.X. Bai, L. Dan, L. Niu, Talanta 85 (2011) 76–81.
[22] Y.J. Guo, L. Deng, J. Li, S.J. Guo, E.R. Wang, S.J. Dong, ACS Nano 5 (2011) 1282–1290.
[23] C.C. Huang, H. Bai, C. Li, G.Q. Shi, Chem. Commun. 47 (2011) 4962–4964.
[24] W.J. Hong, H. Bai, Y.X. Xu, Z.Y. Yao, Z.Z. Gu, G.Q. Shi, J. Phys. Chem. C 114 (2010) 1822–1826.
[25] J. Simplicio, Biochemistry 11 (1972) 2525–2528.
[26] F. Valentini, L. Cristofanelli, M. Carbone, G. Palleschi, Electrochim. Acta 63 (2012) 37–46.
[27] J.B. Xu, T.S. Zhao, L. Zeng, Int. J. Hydrogen Energy 37 (2012) 15976–15982.
[28] R.M. Santos, M.S. Rodrigues, J. Laranjinha, R.M. Barbosa, Biosens. Bioelectron. 44 (2013) 152–159.
[29] Q. Ma, S.Y. Ai, H.S. Yin, Q.P. Chen, T.T. Tang, Electrochim. Acta 55 (2010) 6687–6694.
[30] Q.Y. Chen, D.H. Li, Q.Z. Zhu, H.H. Yang, H. Zheng, J.G. Xu, Anal. Chim. Acta 406 (2000) 209–215.
[31] T. Xue, S. Jiang, Y.Q. Qu, Q. Su, R. Cheng, S. Dubin, C.Y. Chiu, R. Kaner, Y. Huang, X.F. Duan, Angew. Chem. Int. Ed. 51 (2012) 3822–3825.
[32] A.M. Toader, E. Volanschi, Rev. Roum. Chim. 52 (2007) 159–167.
[33] M. Zhang, R. Yuan, Y.Q. Chai, S.H. Chen, X. Zhang, H.A. Zhong, C. Wang, RSC Adv. 2 (2012) 4639–4641.
[34] J. Chen, L. Zhao, H. Bai, G.Q. Shi, J. Electroanal. Chem. 657 (2011) 34–38.
[35] W. Chen, S. Cai, Q.Q. Ren, W. Wen, Y.D. Zhao, Analyst 137 (2010) 49–58.

[36] W.J. Zhao, Z.H. Wang, Q.M. Li, Anal. Methods 4 (2012) 1105–1109.
[37] Y.J. Guo, J. Li, S.J. Dong, Sens. Actuators B 160 (2011) 295–300.
[38] X.Y. Lin, Y.N. Ni, S. Kokot, Anal. Chim. Acta 765 (2013) 54–62.
[39] Z.J. Song, R. Yuan, Y.Q. Chai, B. Yin, P. Fu, J.F. Wang, Electrochim. Acta 55 (2010) 1778–1784.
[40] X.Y. Lin, Y.N. Ni, S. Kokot, J. Hazard. Mater. 243 (2012) 232–241.
[41] E. Jin, X.F. Lu, L.L. Cui, D.M. Chao, C. Wang, Electrochim. Acta 55 (2010) 7230–7234.
[42] W. Chen, S. Cai, Q.Q. Ren, W. Wen, Y.D. Zhao, Analyst 137 (2012) 49–58.